AJNR

Qualitative and Quantitative Performance of 18F-FDG-PET/MRI versus 18F-FDG-PET/CT in Patients with Head and Neck Cancer

S. Partovi, A. Kohan, J.L. Vercher-Conejero, C. Rubbert, S. Margevicius, M.D. Schluchter, C. Gaeta, P. Faulhaber and M.R. Robbin

Qualitative and Quantitative Performance of ^{18}F-FDG-PET/MRI versus ^{18}F-FDG-PET/CT in Patients with Head and Neck Cancer

S. Partovi, A. Kohan, J.L. Vercher-Conejero, C. Rubbert, S. Margevicius, M.D. Schluchter, C. Gaeta, P. Faulhaber, and M.R. Robbin

ABSTRACT

BACKGROUND AND PURPOSE: MR imaging and PET/CT are integrated in the work-up of head and neck cancer patients. The hybrid imaging technology ^{18}F-FDG-PET/MR imaging combining morphological and functional information might be attractive in this patient population. The aim of the study was to compare whole-body ^{18}F-FDG-PET/MR imaging and ^{18}F-FDG-PET/CT in patients with head and neck cancer, both qualitatively in terms of lymph node and distant metastases detection and quantitatively in terms of standardized uptake values measured in ^{18}F-FDG-avid lesions.

MATERIALS AND METHODS: Fourteen patients with head and neck cancer underwent both whole-body PET/CT and PET/MR imaging after a single injection of ^{18}F-FDG. Two groups of readers counted the number of lesions on PET/CT and PET/MR imaging scans. A consensus reading was performed in those cases in which the groups disagreed. Quantitative standardized uptake value measurements were performed by placing spheric ROIs over the lesions in 3 different planes. Weighted and unweighted κ statistics, correlation analysis, and the Wilcoxon signed rank test were used for statistical analysis.

RESULTS: κ statistics for the number of head and neck lesion lesions counted (pooled across regions) revealed interreader agreement between groups 1 and 2 of 0.47 and 0.56, respectively. Intrareader agreement was 0.67 and 0.63. The consensus reading provided an intrareader agreement of 0.63. For the presence or absence of metastasis, interreader agreement was 0.85 and 0.70. The consensus reading provided an intrareader agreement of 0.72. The correlations between the maximum standardized uptake value in ^{18}F-FDG-PET/MR imaging and ^{18}F-FDG-PET/CT for primary tumors and lymph node and metastatic lesions were very high (Spearman $r = 1.00$, 0.93, and 0.92, respectively).

CONCLUSIONS: In patients with head and neck cancer, ^{18}F-FDG-PET/MR imaging and ^{18}F-FDG-PET/CT provide comparable results in the detection of lymph node and distant metastases. Standardized uptake values derived from ^{18}F-FDG-PET/MR imaging can be used reliably in this patient population.

ABBREVIATIONS: SUV = standardized uptake value; SUV$_{max}$ = maximum standardized uptake value

Head and neck cancers are relatively common malignancies in the United States,[1,2] with an incidence estimated between 10 and 20 cases per 100,000 per year.[3] Multimodal complex therapy

protocols are established, which include chemotherapy, radiation therapy, and surgical resection.[4] Accurate staging and re-staging are essential for selection of the appropriate treatment approach in individual patients.

Human whole-body combined or hybrid PET/MR imaging has been recently introduced in the clinical arena. The rationale for PET/MR imaging in head and neck cancer is based on the role of MR imaging and PET/CT in the work-up of this patient population. In head and neck cancer, MR imaging is an attractive technique due to its superior soft-tissue contrast and lower occurrence of metallic dental implant artifacts.[5] PET/CT, however, is capable of depicting regional adenopathy, small tumors, and distant metastases in a whole-body approach. PET/CT is an established technique for staging, re-staging, and treatment-response assessment in head and neck cancer.[6,7] PET/MR imaging, however, might also be attractive for head and neck cancer imaging because it combines the superior soft-tissue and functional

Table 1: Baseline characteristics of patients

Patient	Sex	Age (yr)	Histopathology	Treatment Prior to PET/MRI Study
1	Male	53	Squamous cell carcinoma of the tongue	Radiation therapy and chemotherapy
2	Male	46	Adenocarcinoma of the salivary gland	Chemotherapy
3	Male	66	Squamous cell carcinoma of the tongue	Radiation therapy and chemotherapy
4	Male	67	Squamous cell carcinoma of the oropharynx	Radiation therapy and chemotherapy
5	Male	51	Adenocarcinoma of the salivary gland	Chemotherapy
6	Male	63	Squamous cell carcinoma of the tongue and pharyngeal wall	Radiation therapy and chemotherapy
7	Male	54	Squamous cell carcinoma of the tonsil	No therapy
8	Female	49	Squamous cell carcinoma of the tongue	Radiation therapy and chemotherapy
9	Male	66	Squamous cell carcinoma of the tonsil	Radiation therapy and chemotherapy
10	Male	54	Squamous cell carcinoma of the tonsil	Radiation therapy and chemotherapy
11	Male	57	Squamous cell carcinoma of the tongue	Radiation therapy and chemotherapy
12	Male	42	Squamous cell carcinoma of the tongue	No therapy
13	Male	54	Squamous cell carcinoma of the oropharynx	Radiation therapy and chemotherapy
14	Male	44	Squamous cell carcinoma of the nasopharynx	No therapy

information of MR imaging with the ability of PET to deliver information about metabolism on a cellular level.[8,9]

Uptake of PET tracer can be visualized and quantified by using standardized uptake values (SUVs). Early comparisons of SUVs between PET/MR imaging and PET/CT from our group and others in healthy tissue of oncology patient population have shown good agreement.[10,11] The logical next step is to analyze correlations of SUV in a variety of pathologic conditions in order to use the values derived from PET/MR imaging data reliably in patients for quantification of studies.

The purpose of this prospective study was to systematically analyze lymph node and distant metastases detection qualitatively on whole-body ^{18}F-FDG-PET/MR imaging versus ^{18}F-FDG-PET/CT in patients with head and neck cancer. A further aim of this study was to compare SUVs of ^{18}F-FDG-avid lesions as a quantitative measure of tracer uptake in whole-body ^{18}F-FDG-PET/MR imaging versus ^{18}F-FDG-PET/CT.

MATERIALS AND METHODS
Patient Population
The Health Insurance Portability and Accountability Act–compliant study was approved by the local ethics committee. All patients gave written informed consent before enrollment in the study. Fourteen patients with head and neck cancer (13 men; mean age, 54.7 ± 8.2 years) were included in the study. The baseline characteristics of the patients are listed in Table 1. The patients were referred for a clinically indicated ^{18}F-FDG-PET/CT and then underwent a ^{18}F-FDG-PET/MR imaging. Two of the 14 patients underwent PET/MR imaging first followed by PET/CT. PET/CT was performed 63 ± 6 minutes and PET/MR imaging was conducted 100 ± 34 minutes after ^{18}F-FDG injection. The mean injected dose of ^{18}F-FDG was 11.7 ± 1.4 mCi.

Only patients with head and neck cancer 18 years or older who were referred by their physicians for clinical PET/CT were eligible for the study. All consecutive patients who gave written informed consent were included in the analysis. Exclusion criteria were as follows: 1) patients who were not able to give informed consent (cognitive impairment), 2) pregnant women, 3) implanted metallic or electronic devices, 4) hip or other joint replacements, and 5) a history of kidney disease, with high creatinine levels or a low glomerular filtration rate.

PET/CT Studies
The PET/CT studies were performed, as previously described, according to a standard clinical protocol.[12] In short, a large-bore PET/CT with time-of-flight technology was used (Gemini TF PET/CT; Philips Healthcare, Best, the Netherlands). PET/CT images were acquired in 9–10 bed positions, with 90–120 seconds per bed position. For attenuation-correction and anatomic localization purposes, a low-dose CT protocol without contrast administration was acquired (parameters: 120 kV; 100 mAs; dose modulation; pitch 0.813; slice thickness 5 mm). The overall imaging time for PET/CT was 17 ± 2 minutes.

PET/MR Imaging Studies
^{18}F-FDG-PET/MR imaging was performed on a combined current-generation time-of-flight PET and a 3T MR imaging system (Ingenuity TF PET/MR; Philips Healthcare). PET/MR images were acquired in 9–11 bed positions, with 120–150 seconds per bed position to compensate for radiotracer decay in those cases in which PET/MR imaging was performed after PET/CT. The MR imaging component was performed with an integrated radiofrequency coil and a multistation protocol. In the protocol, the slab size was 6 cm and the maximum FOV was 46 cm. For attenuation correction, a whole-body free-breathing 3D T1-weighted spoiled gradient-echo sequence (sequence parameters: TE, 2.3 ms; TR, 4 ms; 10° flip angle) was acquired. The automatic attenuation-correction procedure was performed according to a previously published method, leading to a 3-segment model with differentiation of air, lung, and soft tissue.[13] The overall time for PET/MR imaging was 29 ± 31 minutes.

Data Analysis
Qualitative reading and quantitative measurements were performed with commercially available software (MIM, Version 5.2; MIM Software, Cleveland, Ohio).

For the qualitative reading, a 2-step approach was used. Initially, 2 independent groups of readers (1 radiologist and 1 nuclear medicine physician per group) read the 28 examinations (14 PET/CT and 14 PET/MR imaging) in a blinded and randomized fashion. After an initial assessment on interreader agreement, a consensus reading was performed in those cases in which the 2 groups disagreed. This second step was also performed in a randomized and blinded fashion
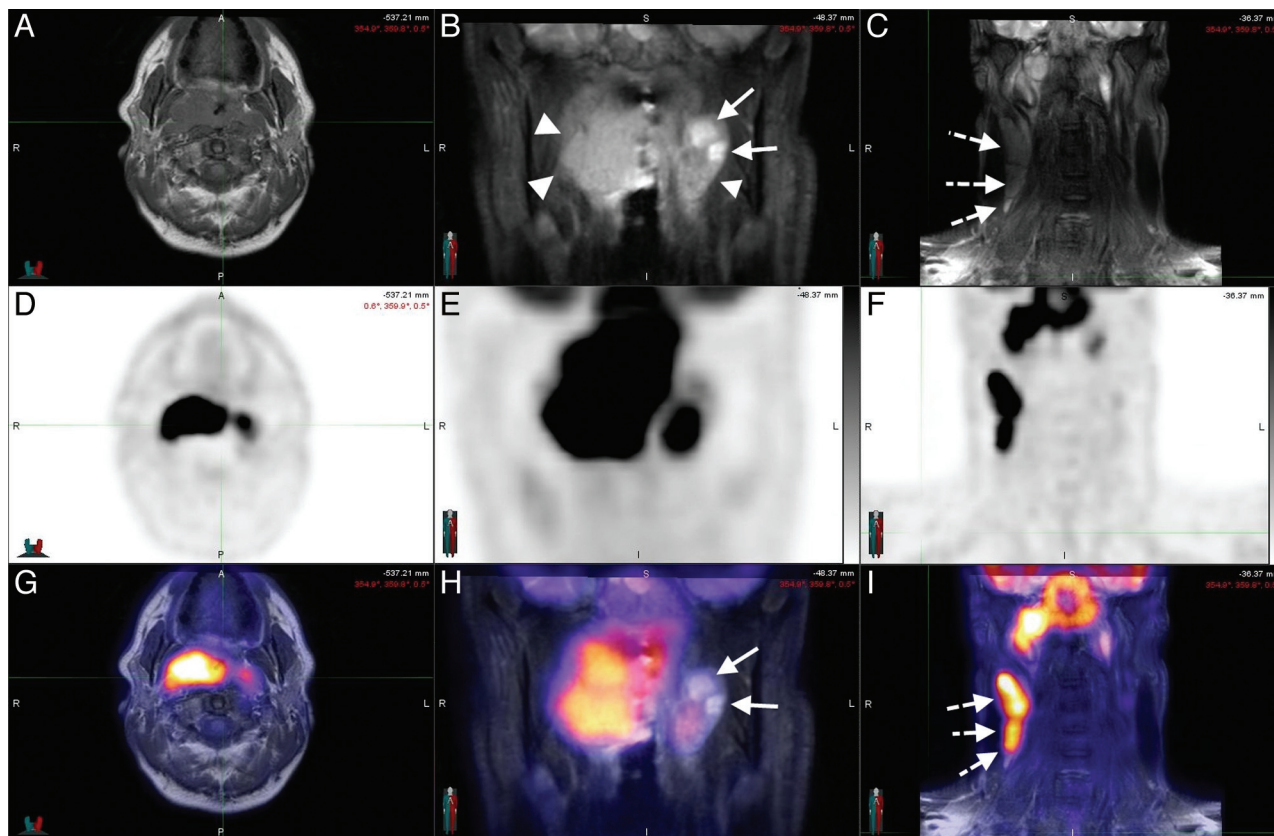
FIG 1. A 44-year-old man with squamous cell carcinoma of the nasopharynx. Axial T1 (*A*) and coronal STIR (*B* and *C*) sequences, with corresponding PET (*D–F*) and the fusion of both (*G–I*), in a patient with nasopharyngeal carcinoma. The neoplastic tissue (*arrowheads*) is easily identifiable in STIR sequences (*B*) in which the cystic component can be visualized (*arrows*). The T1-weighted sequences allow a good assessment of the fat planes. Metastatic lymph nodes (*dotted arrows*) can be assessed morphologically (*C*) and functionally (*I*). Notice the concordance of the cystic areas of the lesion with an area of lower ^{18}F-FDG uptake as expected.

and included 18 examinations, corresponding to 9 patients. Clinical follow-up based on patient charts confirmed the presence or absence of head and neck cancer.

Quantitative analysis of the detected lesions was performed by an experienced board-certified nuclear medicine physician (J.L.V.-C.) through the placement of spheric ROIs over the lesions in 3 different planes (axial, sagittal, and coronal). Maximum SUVs of the lesions, both in PET/CT and PET/MR imaging, were recorded.

Statistical Analysis

Unless otherwise specified, continuous data are reported as mean ± SD. For the first reading, inter- and intrareader agreement was assessed for the number of lesions by using weighted κ statistics. For the first reading, inter- and intrareader agreement was also assessed for the presence or absence of distant metastases (metastases yes or no) by using an unweighted κ statistics. Interreader agreement for PET/CT and PET/MR imaging was evaluated between groups 1 and 2. Intrareader agreements for groups 1 and 2 were evaluated between PET/MR imaging and PET/CT. For the second reading, intrareader agreement for the number of lesions was assessed between PET/MR imaging and PET/CT by using a weighted κ statistics. In this reading, the number of lesions ranged from 0 to 9, and they were categorized as 0, 1, 2, 3, 4, 5 or more. For the second reading, intrareader agreement for the presence or absence of distant metastases (metastases yes or no) was evaluated as well between PET/MR imaging and

PET/CT by using an unweighted κ statistics. For interpretation of the κ statistics, we applied the established criteria of Landis and Koch [14]: κ values in the range of <0.0, 0.0−0.20, 0.21−0.40, 0.41−0.60, 0.61−0.80, and >0.80 represented poor, slight, fair, moderate, substantial, and almost perfect, respectively.

For the assessment of maximum standardized uptake value (SUV_{max}), a clinical (primary tumor, lymph node, and distant metastases) and a localization (for distant metastases: bone, liver, and lung lesions) based assessment were performed. Spearman correlation coefficients between SUV_{max} in PET/MR imaging and PET/CT were calculated. Differences between SUV_{max} in PET/MR imaging and PET/CT were tested by using the Wilcoxon signed rank test. Interpretation of the Spearman correlation coefficients was performed per established standards as previously described[10]: A value ≤0.35 represented a weak correlation; a value between 0.36 and 0.67 represented a moderate correlation; a value between 0.68 and 1.0 represented a high correlation, where a value of ≥0.90 represented a very high correlation. For differences in the Wilcoxon signed rank test, $P < .05$ was considered significant.

RESULTS

Three representative PET/MR imaging cases of head and neck cancer of the study are shown in Fig 1 and On-line Figs 1 and 2.

Qualitative Reading

Agreement on the Number of Lesions (Pooled across Regions). For the first reading, interreader agreements between groups 1 and 2 were moderate for both imaging modalities: Weighted κ values were 0.47 (95% CI, 0.30–0.63) and 0.56 (95% CI, 0.34–0.78) for PET/MR imaging and PET/CT, respectively. For the first reading, intrareader agreements between PET/MR imaging and PET/CT were substantial for both groups: Weighted κ values were 0.67 (95% CI, 0.45–0.88) and 0.63 (95% CI, 0.45–0.80) for groups 1 and 2, respectively.

For the second reading, intrareader agreement between PET/MR imaging and PET/CT was substantial (0–5 or more lesions): The weighted κ was 0.63 (95% CI, 0.47–0.79).

Agreement on the Presence or Absence of Metastases. For the first reading, interreader agreement between groups 1 and 2 was

Table 2: Statistical analysis of differences and correlation between SUV$_{max}$ from PET/CT and PET/MRI

	Primary Tumor Lesions (n = 4)	Lymph Node Lesions (n = 45)	Distant Metastasis Lesions (n = 38)
Spearman r	1.00	0.93	0.92
PET/CT	15.69 ± 8.61	5.42 ± 2.83	5.30 ± 2.56
PET/MRI	15.88 ± 5.01	7.10 ± 3.61	6.35 ± 2.92
Difference[a]	0.20 ± 3.97	1.67 ± 1.76	1.05 ± 1.42
P value[b]	.875	<.0001	<.0001

[a] Difference is SUV$_{max}$ PET/MRI minus SUV$_{max}$ PET/CT.
[b] P value from the Wilcoxon signed rank test.

Table 3: Statistical analysis of differences and correlation between SUV$_{max}$ from PET/CT and PET/MRI regarding the location of distant metastasis

	Bone Lesions (n = 12)	Liver Lesions (n = 9)	Lung Lesions (n = 15)
Spearman r	0.89	0.88	0.93
PET/CT	5.67 ± 2.14	5.92 ± 3.43	4.13 ± 1.41
PET/MRI	6.78 ± 3.28	6.83 ± 2.73	5.12 ± 2.07
Difference[a]	1.11 ± 1.96	0.91 ± 1.56	0.99 ± 0.88
P value[b]	.034	.098	.0006

[a] Difference is SUV$_{max}$ PET/MRI minus SUV$_{max}$ PET/CT.
[b] P value from the Wilcoxon signed rank test.

almost perfect for PET/MR imaging and was substantial for PET/CT: Unweighted κ values were 0.85 (95% CI, 0.56–1.00) and 0.70 (95% CI, 0.33–1.00) for PET/MR imaging and PET/CT, respectively. For the first reading, intrareader agreement between PET/MR imaging and PET/CT was substantial for group 1 and almost perfect for group 2: Unweighted κ values were 0.69 (95% CI, 0.30–1.00) and 0.84 (95% CI, 0.55–1.00) for groups 1 and 2, respectively.

For the second reading, intrareader agreement between PET/MR imaging and PET/CT was substantial: The unweighted κ value was 0.72 (95% CI, 0.38–1.00).

Quantitative Analysis

The statistical analysis of the clinical-based assessment of the SUV$_{max}$ values is shown in Table 2. The scatterplot for visualization of SUV$_{max}$ correlation of ^{18}F-FDG-avid lymph node lesions is shown in Fig 2. Because there were only 4 primary tumors, a scatterplot for the primary tumors was not created. Very high correlations between SUV$_{max}$ in PET/MR imaging and PET/CT could be found for primary tumors and lymph node and metastatic lesions (Spearman r = 1.00, 0.93, and 0.92, respectively). The absolute values were higher in PET/MR imaging compared with PET/CT for primary tumor and lymph node and metastatic lesions. This increase in SUV$_{max}$ for PET/MR imaging versus PET/CT was statistically significant for lymph node and metastatic lesions (P < .0001 for both), whereas the difference did not reach the significance level for the primary tumor lesions (P = .875).

The SUV$_{max}$ values are strongly based on the attenuation-correction maps, and the attenuation-correction maps are dependent on the anatomic location. The primary tumor and the lymph node lesions are both in the head and neck region. Because the metastases are in different anatomic areas, however, a location-based SUV$_{max}$ analysis was performed, and the results are demonstrated in Table 3. The scatterplots for visualization of SUV$_{max}$ correlations of ^{18}F-FDG-avid metastatic lesions in the
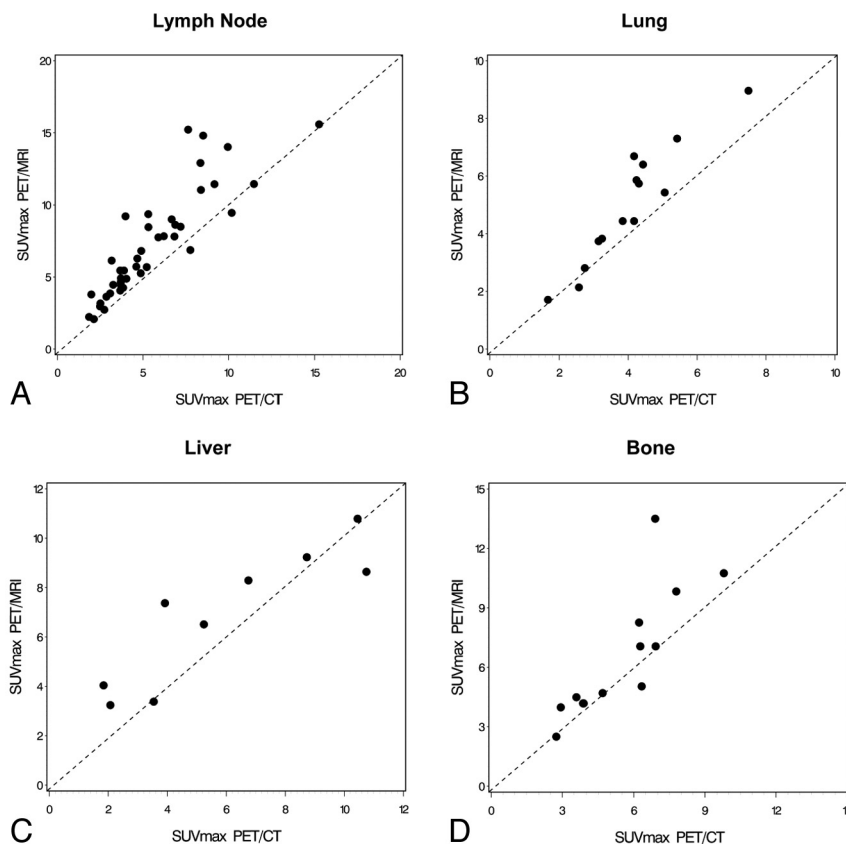

FIG 2. Scatterplots as visualization of the correlations demonstrating SUV$_{max}$ values in PET/CT and PET/MR imaging for ^{18}F-FDG-avid lymph node (A), lung (B), liver (C), and bone (D) lesions.

lung, liver, and bone are shown in Fig 2. High correlations between SUV_{max} in PET/MR imaging and PET/CT could be found for bone and liver lesions (Spearman $r = 0.89$ and 0.88, respectively), whereas a very high correlation was found for lung lesions (Spearman $r = 0.93$). The absolute SUV_{max} values were higher in PET/MR imaging compared with PET/CT for bone, liver, and lung lesions. These increases in SUV_{max} for PET/MR imaging versus PET/CT were statistically significant for bone and lung lesions ($P = .034$ and $P = .0006$, respectively), whereas the difference did not reach the significance level for the liver lesions ($P = .098$).

DISCUSSION

With a dedicated reading session, including radiology and nuclear medicine physicians, detection of lymph node and distant metastases by using whole-body ^{18}F-FDG-PET/MR imaging in patients with head and neck cancer was equal to PET/CT. Regarding the lesion-based analysis, the intrareader agreement was substantial for the first and second readings, and the inter-reader agreement (first reading) was moderate. Regarding the analysis of the presence or absence of metastatic disease, the intrareader agreement for the first and second readings was substantial to almost perfect, and the interreader agreement (first reading) was almost perfect.

Very high correlations between SUV_{max} from ^{18}F-FDG-avid lesions in PET/MR imaging versus PET/CT were found. In the quantitative analysis part, we evaluated SUV correlation per type of lesion (primary tumor or lymph node or distant metastases) and per anatomic localization. As mentioned previously, it is important to conduct a localization-based analysis due to the crucial role of attenuation correction and its dependency on the anatomic region. In both analyses, very high correlations were demonstrated, thus allowing the reliable use of the values in patients with head and neck cancer for quantification of tracer uptake and lesion assessment.

Furthermore, the high number of distant metastases detected demonstrates the crucial role of a whole-body approach for staging and re-staging in this patient population.

PET/MR imaging is promising for head and neck cancer imaging because these tumors frequently require both PET/CT and MR imaging during patient work-up. Evidence from this study and from recently published studies reveals head and neck cancer as one of the future indications for PET/MR imaging.[15]

In one of the initial human feasibility studies with 8 patients with head and neck cancer, the simultaneous PET/MR imaging brain prototype was used after standard-of-care PET/CT imaging.[16] For attenuation correction, a previously published combined atlas registration and pattern-recognition approach was applied.[17] The authors reported an excellent image quality with minor streak artifacts in the PET datasets of PET/MR imaging not affecting the assessment of the malignancy. When comparing the tracer uptake of the tumor in PET/MR imaging versus PET/CT, a higher ^{18}F-FDG uptake was detected in PET/MR imaging. A high correlation coefficient was found for the mean and maximum metabolic ratios of the tumors between both imaging technologies.[16] Our study differs from this early PET/MR imaging feasibility investigation using the brain prototype. This prototype had a limited craniocaudal FOV of 19 cm, hence enabling visualization

only to the level II neck lymph node regions.[16] We used a whole-body approach, which is of clinical relevance in patients with head and neck cancer. According to a screening study in preoperative patients with head and neck cancer, 17% had distant metastatic disease.[18] A whole-body PET/MR imaging approach also helps in visualizing second primary malignancies, which is important in this patient population.[19,20]

A recently published feasibility study using ^{18}F-FDG-PET/MR imaging for initial staging of 20 patients having head and neck squamous cell carcinoma confirmed the possibility of applying the hybrid imaging technology to this patient population without compromising image quality.[21] ^{18}F-FDG-PET/MR imaging was compared, in this study, with a traditional ^{18}F-FDG-PET scanner. Malignancies could be detected with PET/MR imaging, PET alone, and MR imaging alone in 17, 16, and 14 of the 20 cases investigated. Significantly more ^{18}F-FDG-avid lymph nodes were detected in PET/MR imaging versus PET. Furthermore, the SUVs in tumor and the cerebellum were significantly higher when comparing PET/MR imaging versus stand-alone PET.[21] This observation is in accordance with our study in which the absolute SUV_{max} were higher in PET/MR imaging versus PET/CT as well. In comparison with their study, the current study compared whole-body ^{18}F-FDG-PET/MR imaging versus ^{18}F-FDG-PET/CT instead of a stand-alone PET. We included, in this study, the 2 most common histopathologic types of head and neck cancer, namely squamous cell carcinoma and adenocarcinoma.

Absolute SUV_{max} values were higher in PET/MR imaging compared with PET/CT. The higher SUV_{max} reached statistical significance in the lymph node and metastatic lesions. In primary tumors, the SUV difference was minimal, not reaching statistical significance, but this can be explained by the small number of primary lesions ($n = 4$) and thus low statistical power. When analyzing the metastatic lesions per region, again this study found higher SUV_{max} in PET/MR imaging versus PET/CT, reaching statistical significance for bone and lung but not liver lesions. We explain the results by the measurement of PET/MR imaging after PET/CT in most patients (12 of 14) leading to an increased tracer uptake with time. However, different attenuation-correction techniques may also contribute to these findings. With regard to the SUV analysis, it is crucial to do correlative studies between PET/MR imaging and PET/CT. In the previously published study of our group comparing SUVs from ^{18}F-FDG-PET/MR imaging with ^{18}F-FDG-PET/CT in healthy tissue, high correlations for SUV_{max} and SUV_{mean} were found.[10] In certain tissues, the absolute SUV_{max} and SUV_{mean} differed significantly, but when a good correlation was shown between PET/MR imaging and PET/CT as the standard method, the values from PET/MR imaging could be used reliably in the clinical settings for follow-up comparisons. Attenuation-correction solutions based on MR imaging data are one of the major challenges for PET/MR imaging.[22] Attenuation correction has an impact on both SUV_{max} and SUV_{mean}.

According to our experience with PET/MR imaging, workflow and associated time constraints frequently pose a challenge in PET/MR imaging. In this study, the PET/CT examination lasted 17 ± 2 minutes and the PET/MR imaging study took 29 ± 31 minutes. This study and others demonstrate that that the scan-

ning time in PET/MR imaging is slightly longer compared with PET/CT.[21] This may change in the future when a full diagnostic MR imaging protocol is integrated into the PET/MR imaging workflow.

The study has limitations. First, only 14 patients with head and neck cancer were enrolled in this prospective study. Second, we did not have a uniform diagnostic MR imaging protocol. Besides the whole-body T1-weighted sequence for attenuation correction, we acquired, in 12 of the 14 patients, extra MR images, but the protocol was not unified. Third, the first 12 of the 14 patients with head and neck cancer underwent PET/CT, followed by PET/MR imaging. Only the last 2 patients had PET/MR imaging first. A randomization approach during the entire study would have been better from a scientific perspective, but when we started the clinical PET/MR imaging program, we decided, due to ethical reasons, to give the clinically referred PET/CT examination priority, followed by the PET/MR imaging study.

CONCLUSIONS

The detection of adenopathy and distant metastatic disease is reliable with whole-body ^{18}F-FDG-PET/MR imaging compared with state-of-the art ^{18}F-FDG-PET/CT imaging in head and neck cancer. This is reflected by the moderate-to-substantial inter- and intrareader agreements with regard to head and neck lesion detection (pooled across regions) and by the substantial to almost perfect inter- and intrareader agreements with regard to detection of the presence or absence of metastatic disease. Very high correlations between SUVs in PET/MR imaging versus PET/CT of ^{18}F-FDG-avid lesions were demonstrated, thus enabling the reliable use of SUVs in this patient population. Head and neck cancer is one of the promising indications for PET/MR imaging.

REFERENCES

1. Ferlay J, Shin HR, Bray F, et al. **Estimates of worldwide burden of cancer in 2008: GLOBOCAN 2008.** *Int J Cancer* 2010;127:2893–917
2. Curado MP, Hashibe M. **Recent changes in the epidemiology of head and neck cancer.** *Curr Opin Oncol* 2009;21:194–200
3. Guntinas-Lichius O, Wendt T, Buentzel J, et al. **Head and neck cancer in Germany: a site-specific analysis of survival of the Thuringian cancer registration database.** *J Cancer Res Clin Oncol* 2010;136:55–63
4. Tulunay-Ugur OE, McClinton C, Young Z, et al. **Functional outcomes of chemoradiation in patients with head and neck cancer.** *Otolaryngol Head Neck Surg* 2013;148:64–68
5. Eiber M, Souvatzoglou M, Pickhard A, et al. **Simulation of a MR-PET protocol for staging of head-and-neck cancer including Dixon MR for attenuation correction.** *Eur J Radiol* 2012;81:2658–65
6. Ishikita T, Oriuchi N, Higuchi T, et al. **Additional value of integrated PET/CT over PET alone in the initial staging and follow up of head and neck malignancy.** *Ann Nucl Med* 2010;42:77–82
7. Iyer NG, Clark JR, Singham S, et al. **Role of pretreatment 18FDG-PET/CT in surgical decision-making for head and neck cancers.** *Head Neck* 2010;32:1202–08
8. Jeong HS, Baek CH, Son YI, et al. **Use of integrated [18F]-FDG PET/CT to improve the accuracy of initial cervical nodal evaluation in patients with head and neck squamous cell carcinoma.** *Head Neck* 2007;29:203–10
9. Ng SH, Yen TC, Chang JT, et al. **Prospective study of [18F]fluoro-deoxyglucose positron emission tomography and computed tomography and magnetic resonance imaging in oral cavity squamous cell carcinoma with palpably negative neck.** *J Clin Oncol* 2006;24:4371–76
10. Kershah S, Partovi S, Traughber BJ, et al. **Comparison of standardized uptake values in normal structures between PET/CT and PET/MRI in an oncology patient population.** *Mol Imaging Biol* 2013;15:776–85
11. Heusch P, Buchbender C, Beiderwellen K, et al. **Standardized uptake values for [18F] FDG in normal organ tissues: comparison of whole-body PET/CT and PET/MRI.** *Eur J Radiol* 2013;82:870–76
12. Partovi S, Kohan A, Gaeta C, et al. **Image quality assessment of automatic three-segment MR attenuation correction vs. CT attenuation correction.** *Am J Nucl Med Mol Imaging* 2013;3:291–99
13. Schulz V, Torres-Espallardo I, Renisch S, et al. **Automatic, three-segment, MR-based attenuation correction for whole-body PET/MR data.** *Eur J Nucl Med Mol Imaging* 2011;38:138–52
14. Landis JR, Koch GG. **The measurement of observer agreement for categorical data.** *Biometrics* 1977;33:159–74
15. Buchbender C, Heusner TA, Lauenstein TC, et al. **Oncologic PET/MRI. Part 1. Tumors of the brain, head and neck, chest, abdomen, and pelvis.** *J Nucl Med* 2012;53:928–38
16. Boss A, Stegger L, Bisdas S, et al. **Feasibility of simultaneous PET/MR imaging in the head and upper neck area.** *Eur Radiol* 2011;21:1439–46
17. Hofmann M, Steinke F, Scheel V, et al. **MRI-based attenuation correction for PET/MRI: a novel approach combining pattern recognition and atlas registration.** *J Nucl Med* 2008;49:1875–83
18. de Bree R, Deurloo EE, Snow GB, et al. **Screening for distant metastases in patients with head and neck cancer.** *Laryngoscope* 2000;110(pt 1):397–401
19. Jones AS, Morar P, Phillips DE, et al. **Second primary tumors in patients with head and neck squamous cell carcinoma.** *Cancer* 1995;75:1343–53
20. Priante AV, Castilho EC, Kowalski LP. **Second primary tumors in patients with head and neck cancer.** *Curr Oncol Rep* 2011;13:132–37
21. Platzek I, Beuthien-Baumann B, Schneider M, et al. **PET/MRI in head and neck cancer: initial experience.** *Eur J Nucl Med Mol Imaging* 2013;40:6–11
22. Keereman V, Mollet P, Berker Y, et al. **Challenges and current methods for attenuation correction in PET/MR.** *MAGMA* 2013;26:81–98